On-Surface Synthesis

On-Surface Synthesis of Polyphenylene Wires Comprising Rigid Aliphatic Bicyclo[1.1.1]Pentane Isolator Units

Biao Yang[+],* Kaifeng Niu[+], Nan Cao, Nitika Grover, Wenchao Zhao, Alexander Riss, Jonas Björk,* Willi Auwärter, Johannes V. Barth,* and Mathias O. Senge*

Dedicated to Professor Henning Hopf

Abstract: Bicyclo[1.1.1]pentane (BCP) motifs are of growing importance to the pharmaceutical industry as sp^3-rich bioisosteres of benzene rings and as molecular building blocks in materials science. Herein we explore the behavior of 1,3-disubstituted BCP moieties on metal surfaces by combining low-temperature scanning tunneling microscopy / non-contact atomic force microscopy studies with density functional theory modeling. We examine the configuration of individual BCP-containing precursors on Au(111), their supramolecular assembly and thermally activated dehalogenative coupling reactions, affording polymeric chains with incorporated electronically isolating units. Our studies not only provide the first sub-molecular insights of the BCP scaffold behavior on surfaces, but also extend the potential application of BCP derivatives towards integration in custom-designed surface architectures.

[*] Dr. B. Yang,[+] Prof. Dr. M. O. Senge
Institute for Advanced Study (TUM-IAS), Focus Group—Molecular and Interfacial Engineering of Organic Nanosystems, Technical University of Munich
Lichtenberg Str. 2a, 85748 Garching (Germany)
E-mail: biao.yang@tum.de
           mathias.senge@tum.de
Homepage: http://www.sengegroup.eu/
              https://www.ias.tum.de/active-fellows/senge-mathias/

Dr. B. Yang,[+] N. Cao, W. Zhao, A. Riss, Prof. Dr. W. Auwärter, Prof. Dr. J. V. Barth
Physics Department E20, Technical University of Munich
James Franck Straße 1, 85748 Garching (Germany)
E-mail: jvb@tum.de

K. Niu,[+] Prof. Dr. J. Björk
Department of Physics, Chemistry and Biology, IFM, Linköping University
58183 Linköping (Sweden)
E-mail: jonas.bjork@liu.se

Dr. N. Grover
School of Chemistry, Chair of Organic Chemistry, Trinity Biomedical Sciences Institute, Trinity College Dublin, The University of Dublin
152–160 Pearse Street, Dublin 2 (Ireland)

[+] These authors contributed equally to this work.

Introduction

Bicyclo[1.1.1]pentane (BCP),[1] as a sp^3-rich bioisostere of an benzene ring, is becoming an appealing functional unit in drug discovery and materials science.[2] It has been shown that replacement of an aromatic ring with the similar-size and conformationally rigid all-sp^3-C BCP scaffold often results in more favorable pharmacokinetic properties, such as increased solubility and higher metabolic stability.[3] With the efforts of synthetic chemists, well-established approaches have been developed to furnish 1,3-disubstituted BCP derivatives,[4] extending to surrogates for 1,4-disubstituted arenes, *tert*-butyl groups, and alkynes in material sciences as linear linkers.[3, 4c, 5] As members of the nonconjugated rigid hydrocarbons (NRHs), their usage in linking functionalities enables the modification of traditional materials in a defined spatial manner,[6] notably by interrupting electric conductivity and providing organic resistor or isolator units.[7] Ultimately, the realization and application of these functions depends on the understanding of interactions and reactivity of the BCP moiety at the molecular level.[8]

Molecular engineering on surfaces[9] is often conducted under ultrahigh vacuum conditions at well-defined substrates. Notably, so-called on-surface synthesis aims at controlling individual adsorbed molecules and their interactions to guide chemical transformations and distinct bond formations.[10] Thus new surface chemistry and bottom-up construction of functional nanostructures becomes possible.[11] To date, studies predominantly focus on flat aromatic precursor species affording planar nanostructures.[12] The only examples of three-dimensional (3D) nonconjugated rigid hydrocarbons studied on surfaces are diamondoids,[13] iptycenes,[14] and [3.3.3]propellanes.[15]

Here we report the first real-space characterization of a 1,3-disubstituted BCP derivative on metal surfaces with low-temperature (LT) scanning tunneling microscopy (STM) and non-contact atomic force microscopy (nc-AFM). Using 1,3-bis(4-iodophenyl)bicyclo[1.1.1]pentane (IPBCP) as precursor,[4c,16] we monitor self-assembly and the thermally activated deiodination coupling reaction on the Au(111) surface, incorporating the BCP scaffold in supramolecular islands and polyphenylene chains. By combining computational modeling using density functional theory (DFT) with STM and AFM image simulations, we successfully identify the conformation and electronic features of molecular nanostructures obtained with BCP scaffolds. Our studies provide

a fundamental understanding of BCP behavior on surfaces and extend on-surface chemistry to 3D isosteres.

Results and Discussion

As shown in Figure 1a, the 1,3-bis(4-iodophenyl) substituted BCP compound is a linear species with an extended carbon backbone.[8,16c] The DFT optimized structure reveals a single species with a 14.69 Å iodine–iodine distance along the molecular axis. After depositing small amounts on Au(111) at low temperature (120 K) individual molecules were found, facilitating the characterization of the pristine adsorption configuration of IPBCP via in situ submolecular-level imaging. Figure 1b and 1c show the corresponding STM and AFM data, recorded at 5 K with a CO functionalized tip.[17] The two images obtained of the same monomer show the clear appearance of a flat-lying species with distinct molecular subunits. In the STM image (Figure 1b) IPBCP features a symmetric linear shape, with three sphere-like protrusions. The measured distance between the two terminal spheres is 14.8 ± 0.2 Å, and the bright center reflects a protruding BCP moiety. STM data reflecting contours of local density of states[18] are not sufficient to infer the detailed adsorption configuration, especially regarding the BCP scaffold conformation with respect to the phenylene substituents and the substrate atomic lattice. With high-resolution AFM observations, detecting frequency shifts induced by short-range repulsive interactions,[19] bond-resolved imaging is possible.[20] Particularly, scans at different imaging heights offer thorough understanding of the configuration and orientation of 3D aliphatic moieties.[21]

AFM images of the same molecule as in Figure 1b were obtained at a series of tip-sample distances. The contrast changes significantly when the CO-tip approaches the sample surface (cf. Figure S1). Initially, the data reveal a small bright oval protrusion at the center, attributed to the BCP core. When approaching the surface step by step the contours of the phenyl rings and iodine on both sides can be distinguished. Simultaneously, the BCP core becomes faint, as shown in Figure 1c. Hereby the phenyl units take a rather flat configuration slightly bent from the higher BCP center to the lower iodine ends. Both rings tilt to the same side with respect to the molecular axis. Interestingly, for the iodine region AFM images show small spots besides the phenylene features, different from the large protrusion in STM data (Figure 1b). Also, the measured distance between the two spots of 16.8 ± 0.2 Å markedly exceeds the model I··I distance, indicating that they do not correspond to iodine atom positions; this could reflect imaging distortions due to the tip CO tip response or the σ-hole influence arising from the uneven charge distribution at halogen atoms.[22]

To better understand the molecular configuration and STM / AFM characteristics, the positioning of the BCP core requires detailed consideration. Accordingly, we performed systematic DFT calculations, indicating four stable adsorption configurations of the monomer, distinguishable by BCP core and phenyl ring orientation. As seen in Figure S2, one BCP methylene unit can face either towards the vacuum (*Config. 1*) or the surface (*Config. 2*) and the molecular phenyl rings can tilt in opposite (*Config. a*) or the same direction (*Config. s*). Comparing the adsorption energies of the optimized systems, the BCP core favors the configuration with two CH_2 units facing towards the surface and the remaining methylene unit pointing to the vacuum. Note that, based on the computational modelling there is no strong preference regarding the rotation of phenyl rings. Since the high-resolution AFM image (Figure 1c) indicates
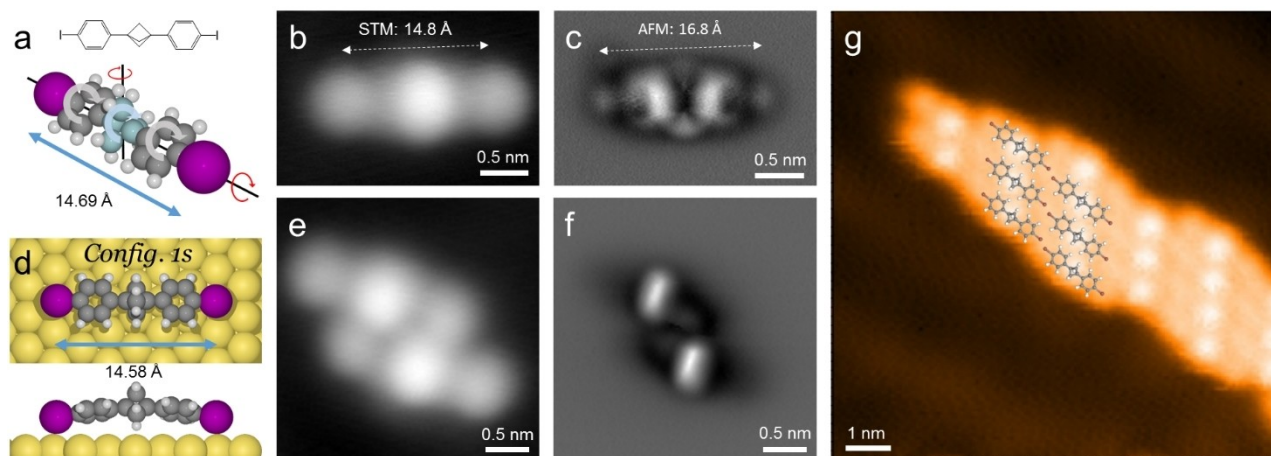

Figure 1. Adsorption and self-assembly of IPBCP on Au(111) at 120 K. a) The chemical structure and optimized model of an IPBCP monomer, exhibiting a 14.69 Å iodine–iodine distance along the molecular axis. b), c) High-resolution STM and nc-AFM images of a single adsorbed IPBCP. The measured distances of the two terminal protrusions are 14.8 ± 0.2 Å and 16.8 ± 0.2 Å, respectively. d) Optimized model of adsorbed IPBCP monomer, exhibiting a 14.58 Å projected iodine–iodine distance. c) H, I, and Au atoms are represented by the grey, white, purple, and yellow spheres, respectively. e), f) High resolution STM and nc-AFM images of two adjacent IPBCP molecules. The AFM scan height is relatively high to resolve the two rigid BCP cores. g) Representative assembly structure of IPBCP when increasing the surface coverage, with the structural models partially overlapped on the STM image. Measurement parameters: b) and e) $I_t = 10$ pA, $V_s = 100$ mV; g) $I_t = 50$ pA, $V_s = -100$ mV; c) and f) $V_s = -2$ mV, constant height.

phenyl rings with the same orientation, *Config. 1s* as shown in Figure 1d is chosen as best model. The calculated projected iodine-iodine distance is 14.58 Å, whereby comprehensive STM and AFM simulations based on the favored configuration give good agreement with the experiments (Figure S3 and S4).

Increasing the molecular coverage at low temperature (120 K) results in the aggregation of small islands stabilized via halogen bonds (Figure S5a), whereby the individual molecules are easily distinguishable in STM data (Figure S5b–d). Moreover, terminal iodine is easily abstracted by applying bias pulses with the STM tip positioned at the molecular periphery (Figure S5e–f), indicating a weak stability of aryl iodide on Au(111), as expected from previous experiments and theory.[23] As STM and nc-AFM images of the dimeric units in aggregates demonstrate the same lateral intermolecular arrangement (see Figure 1e and f), there is obviously no direct contact between adjacent BCP cores. Thus, halogen bonding and weak van der Waals lateral interaction leads to the narrow arrays following the surface chevron reconstruction (cf. Figure 1g).

Thermal treatment of the as-deposited sample above room temperature triggers dehalogenation and subsequent coupling reaction between monomers (Figure S6). Annealing at 375 K for 10 minutes, drives a phase transformation from small islands to more extended domains. As shown in Figure 2a, they contain regular chains with 12.2 ± 0.1 Å periodi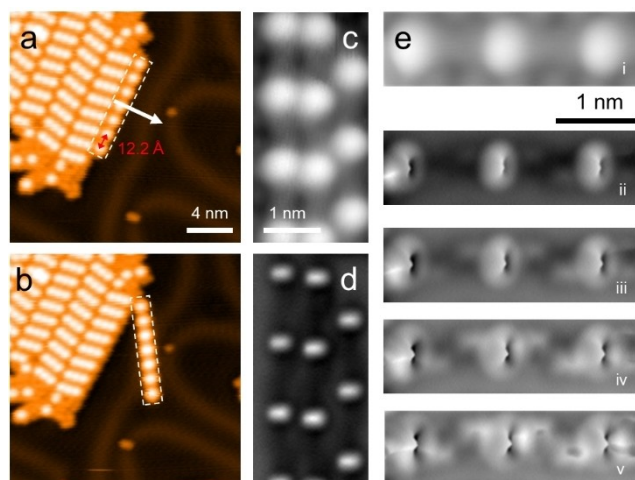city, easily discernible by the sequential arrangement of bright BCP cores. This observation agrees well with the theoretical calculations, in which the periodicity was calculated as 12.07 Å in gas phase. Besides such distinct chains isolated by rows of iodine atoms, patches with merged chains arranged side by side with a slight offset of incorporated BCP cores exist. In order to unravel the nature of connections within the chains, molecular manipulation experiments using the STM tip were conducted. Figures 2a,b show lateral manipulation of a chain featuring seven BCP units at the edge of an island. The entire chain can be moved away without its shape or length affected. More molecular manipulation experiments and detailed STM observations (Figure S7) confirmed the integrity and rigidity of the chains, indicating robust connections between the constituents.

To further distinguish the connection motif of the polymers obtained, we recorded high-resolution STM and AFM data of three chain segments, as shown in Figure 2c and d, respectively. While the STM image shows seamless morphology between bright BCP cores along the chain directions, the AFM image, which probes the rigid BCP core at higher tip-sample distance, shows a rectangular protrusion, indicating the orientation of the phenylene ring on both sides. Upon closer inspection of a trimer segment along the chain a covalent connection, reflecting C–C coupling of deiodinated units, becomes clearly evident (Figure 2e).

STM data of a covalent dimer segment comprising two BCP linked by a biphenylene bridge are reproduced in Figure 3a. The corresponding AFM images at different tip heights (Figure 3b and c) exhibit shapes of BCP cores reminiscent of those in monomers (Figure S1). To further clarify the configuration of this covalent chain, DFT calculations of dimer model systems were performed. Similar to the monomeric bonding, the adsorption configurations of covalent chains exhibit two possible orientations
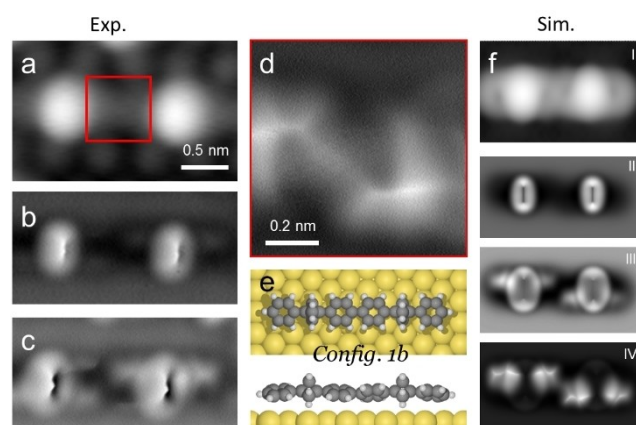

Figure 2. 1D covalent chains formed on Au(111) upon thermal treatment (375 K) of pre-deposited IPBCP. a) and b) STM images before and after tip manipulation on an island of covalent chains. The white arrow in (a) indicates the path of tip during manipulation (tip-sample distance is defined at tunneling condition of $I_t = 1$ nA, $V_s = 3$ mV with the tip placed above the chain (dashed rectangular; the tip was then moved with a speed of 100 pm s^{-1} in the constant height mode). c) STM and d) AFM images of a same frame with three chain segments. The AFM image is taken at a larger tip-sample distance and shows bright protrusions at the positions of the rigid BCP. e) STM and height-dependent AFM inspections of a trimer segment along the covalent chain. Measurement parameters: a) $I_t = 100$ pA, $V_s = -500$ mV; b) $I_t = 20$ pA, $V_s = -500$ mV; c) and e$_i$) $I_t = 10$ pA, $V_s = 100$ mV; d) and e$_{ii-v}$) $V_s = 0$ V, constant height.

Figure 3. Determination of the adsorption configuration of the covalent chains. a) Experimental STM image of a dimer. b) and c) AFM images at different tip sample height of the same dimer frame as (a). d) Bond-resolved AFM image of the biphenylene linker as indicated by the red square in a). e) The optimized *Config. 1b* model of a covalent dimer on Au(111). f) Simulated STM (I) and AFM (II–IV) images based on the model in (e). Measurement parameters: a) $I_t = 10$ pA, $V_s = 200$ mV; b)–d) $V_s = 0$ V, constant height.

of the BCP core and tilted phenyl rings with a higher degree of freedom (Figure S10). Importantly, the dominant factor of the adsorption geometry is the BCP orientation, whereby *Config. 1* is energetically favored (adsorption energies in the -2.27 to 2.13 eV range) with two CH_2 facing towards the surface and the remaining CH_2 pointing to vacuum. The connected aromatic units are tilted alternately (Figure S10), in agreement with AFM observations (Figure 2e and S8, S9). Thus, combining the experimental evidence with DFT calculations we confidently identify the *Config. 1* with alternately tilted biphenyl units (*Config. 1b*) as optimal adsorption configuration depicted in Figure 3e. Moreover, the corresponding STM and AFM simulations (Figure S11–13) compare well with the experimental images, further corroborating our model of a 1D covalent polymer, designated poly-PBCP, with connections of phenylene termini.[24]

Creating large sets of 1D polymers facilitates easy characterization and materials application. Free iodine atoms sometimes slip between the formed covalent chains, leading to disordered patches. However, by extended annealing we can steer the regular arrangement of 1D chains at the mesoscale (cf. Figure 4, S14). As illustrated by the STM image in Figure 4a, the covalent chains are arranged next to each other, with BCP protrusions placed regularly. In a theoretical framework, the 1D poly-PBCP polymers can be described as polyphenylene (poly-P) chains with BCP scaffolds replacing every third phenylene unit. Accordingly, a direct comparison of polyphenylene electronic properties with and without BCP units is straightforward. For free-standing linear chains, the optimized period (12.07 Å) in poly-PBCP is somewhat shorter than that of a terphenyl segment in poly-P (13.08 Å). Hereby the calculated band gap between the highest occupied electronic band and the lowest unoccupied band of poly-PBCP and poly-P is markedly different, with poly-PBCP exhibiting a 1.12 eV larger band gap (2.98 vs 1.86 eV, cf. Figure S15), which reflects the electronic properties of the incorporated BCP units and indicates the utility of this scaffold as resistor/isolator units in molecular electronics using all-carbon modules.
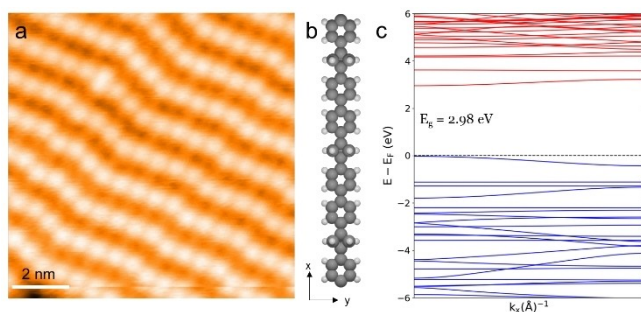
It should be noted that semi-local DFT calculations may severely underestimate band gaps, and the underlying metal surface will also affect the electronic structure of the system. We performed direct measurement of the expected band gap region by scanning tunneling spectroscopy (STS, dI/dV) along poly-PBCP chains (cf. Figure S16). However, in the accessible experimental bias range of -2.0 to $+2.0$ V, no clear band onsets are observed, indicating hybridization effects (frequently encountered for the lowest occupied molecular orbitals or valence band with related systems on metal substrates), or an experimental band gap exceeding 4.0 eV.

To explore the thermal stability, we further annealed the poly-PBCP sample at higher temperature. However, changes occurred upon annealing treatment above 420 K and resulted in decomposition of the periodic structure and formation of fused four-[25] and five-membered ring structures (Figures S17 to S20). This result is somewhat unexpected because of the reported higher stability of either biphenylene or BCP unit. However, examples of metals such as Au, Ir, Rh acting as catalysts for the rearrangement of small rigid molecules are known.[26]

Conclusion

We performed a real-space characterization of a BCP-containing derivative on a well-defined metal surface with state-of-the-art LT-STM and nc-AFM techniques. For the employed IPBCP precursor, we characterized adsorption, self-assembly and thermally activated deiodination coupling reaction Au(111), affording polyphenylene chains with regularly placed BCP scaffolds. Combined with DFT modeling, as well as STM and AFM simulations, we successfully identified the characteristic structural, conformational and electronic features. Our systematic multi-technique study provides a fundamental understanding of BCP derivatives on surfaces and extends the scope of on-surface synthesis to 3D isosteres. Bicyclo[1.1.1]pentane scaffolds are identified as versatile resistor/isolator units in molecular nanostructures at surfaces, opening novel avenues for the exploration of further aspects and tunability in organic electronics, e.g., via incorporation of tetrapyrroles or other functional units.[27]

Figure 4. a) STM image of the long-range ordered assembly of covalent chains. b) Gas phase optimized model of the poly-PBCP chain. c) DFT calculated band structure of the poly-PBCP chain, showing an energy gap of 2.98 eV. Measurement parameters: a) $I_t = 100$ pA, $V_s = -10$ mV.

Conflict of Interest

The authors declare no conflict of interest.

Data Availability Statement

The data that support the findings of this study are available from the corresponding author upon reasonable request.

[1] K. B. Wiberg, F. H. Walker, *J. Am. Chem. Soc.* **1982**, *104*, 5239–5240.

[2] a) G. M. Locke, S. S. R. Bernhard, M. O. Senge, *Chem. Eur. J.* **2019**, *25*, 4590–4647; b) P. K. Mykhailiuk, *Org. Biomol. Chem.* **2019**, *17*, 2839–2849.

[3] A. F. Stepan, C. Subramanyam, I. V. Efremov, J. K. Dutra, T. J. O'Sullivan, K. J. DiRico, W. S. McDonald, A. Won, P. H. Dorff, C. E. Nolan, S. L. Becker, L. R. Pustilnik, D. R. Riddell, G. W. Kauffman, B. L. Kormos, L. M. Zhang, Y. S. Lu, S. H. Capetta, M. E. Green, K. Karki, E. Sibley, K. P. Atchison, A. J. Hallgren, C. E. Oborski, A. E. Robshaw, B. Sneed, C. J. O'Donnell, *J. Med. Chem.* **2012**, *55*, 3414–3424.

[4] a) P. Kaszynski, J. Michl, *J. Org. Chem.* **1988**, *53*, 4593–4594; b) R. Gianatassio, J. M. Lopchuk, J. Wang, C. M. Pan, L. R. Malins, L. Prieto, T. A. Brandt, M. R. Collins, G. M. Gallego, N. W. Sach, J. E. Spangler, H. C. Zhu, J. J. Zhu, P. S. Baran, *Science* **2016**, *351*, 241–246; c) I. S. Makarov, C. E. Brocklehurst, K. Karaghiosoff, G. Koch, P. Knochel, *Angew. Chem. Int. Ed.* **2017**, *56*, 12774–12777; d) N. Grover, M. O. Senge, *Synthesis* **2020**, *52*, 3295–3325.

[5] a) J. Kanazawa, K. Maedam, M. Uchiyama, *J. Am. Chem. Soc.* **2017**, *139*, 17791–17794; b) V. K. Vyas, G. J. Clarkson, M. Wills, *Org. Lett.* **2021**, *23*, 3179–3183.

[6] a) S. S. R. Bernhard, G. M. Locke, S. Plunkett, A. Meindl, K. J. Flanagan, M. O. Senge, *Chem. Eur. J.* **2018**, *24*, 1026–1030; b) A. D. Dharma, C. Chen, L. K. MacReadie, *Aust. J. Chem.* **2022**, *75*, 155–159.

[7] a) D. K. Lavallee, B. Anderes, *Inorg. Chim. Acta* **1983**, *79*, 213–214; b) D. N. Beratan, *J. Am. Chem. Soc.* **1986**, *108*, 4321–4326; c) K. Kilså, J. Kajanus, A. N. MacPherson, J. Mårtensson, B. Albinsson, *J. Am. Chem. Soc.* **2001**, *123*, 3069–3080.

[8] N. Grover, K. J. Flanagan, C. Trujillo, C. J. Kingsbury, M. O. Senge, *Eur. J. Org. Chem.* **2020**, 1113–1122.

[9] a) P. A. Held, H. Fuchs, A. Studer, *Chem. Eur. J.* **2017**, *23*, 5874–5892; b) L. Grill, M. Dyer, L. Lafferentz, M. Persson, M. V. Peters, S. Hecht, *Nat. Nanotechnol.* **2007**, *2*, 687–691; c) L. Grill, S. Hecht, *Nat. Chem.* **2020**, *12*, 115–130.

[10] S. Clair, D. G. de Oteyza, *Chem. Rev.* **2019**, *119*, 4717–4776.

[11] a) J. V. Barth, G. Constantini, K. Kern, *Nature* **2005**, *437*, 671–679; b) J. Cai, P. Ruffieux, R. Jaafar, M. Bieri, T. Braun, S. Blankenburg, M. Muoth, A. P. Seitsonen, M. Saleh, X. Feng, K. Muellen, R. Fasel, *Nature* **2010**, *466*, 470–473.

[12] a) Q. Sun, R. Zhang, J. Qiu, R. Liu, W. Xu, *Adv. Mater.* **2018**, *30*, 1705630; b) J. Su, M. Telychko, S. Song, J. Lu, *Angew. Chem. Int. Ed.* **2020**, *59*, 7658–7668; c) Y. Jin, Y. Hu, M. Ortiz, S. Huang, Y. Ge, W. Zhang, *Chem. Soc. Rev.* **2020**, *49*, 4637–4666.

[13] a) H.-Y. Gao, M. Šekutor, L. Liu, A. Timmer, H. Schreyer, H. Mönig, S. Amirjalayer, N. A. Fokina, A. Studer, P. R. Schreiner, H. Fuchs, *J. Am. Chem. Soc.* **2019**, *141*, 315–322; b) K. Feng, E. Solel, P. R. Schreiner, H. Fuchs, H.-Y. Gao, *J. Phys. Chem. Lett.* **2021**, *12*, 3468–3475.

[14] a) L. Grossmann, B. T. King, S. Reichlmaier, N. Hartmann, J. Rosen, W. M. Heckl, J. Björk, M. Lackinger, *Nat. Chem.* **2021**, *13*, 730–736; b) S. Kawai, O. Krejčí, T. Nishiuchi, K. Sahara, T. Kodama, R. Pawlak, E. Meyer, T. Kubo, A. S. Foster, *Sci. Adv.* **2020**, *6*, eaay8913.

[15] S. Kawai, T. Nishiuchi, T. Kodama, P. Spijker, R. Pawlak, T. Meier, J. Tracey, T. Kubo, E. Meyer, A. S. Foster, *Sci. Adv.* **2017**, *3*, e1603258.

[16] a) A. de Meijere, L. Zhao, V. N. Belov, M. Bossi, M. Noltemeyer, S. W. Hell, *Chem. Eur. J.* **2007**, *13*, 2503–2516; b) E. Sitte, B. Twamley, N. Grover, M. O. Senge, *J. Org. Chem.* **2021**, *86*, 238–1245; c) J. L. Adcock, A. A. Gakh, J. L. Pollitte, C. Woods, *J. Am. Chem. Soc.* **1992**, *114*, 3980–3981.

[17] L. Gross, F. Mohn, N. Moll, P. Liljeroth, G. Meyer, *Science* **2009**, *325*, 1110–1114.

[18] G. Binnig, H. Rohrer, C. Gerber, E. Weibel, *Appl. Phys. Lett.* **1982**, *40*, 178–180.

[19] F. J. Giessibl, *Rev. Mod. Phys.* **2003**, *75*, 949–983.

[20] L. Gross, F. Mohn, N. Moll, B. Schuler, A. Criado, E. Guitian, D. Pena, A. Gourdon, G. Meyer, *Science* **2012**, *337*, 1326–1329.

[21] a) D. Ebeling, M. Šekutor, M. Stiefermann, J. Tschakert, J. E. P. Dahl, R. M. K. Carlson, A. Schirmeisen, P. R. Schreiner, *ACS Nano* **2017**, *11*, 9459–9466; b) D. Ebeling, M. Šekutor, M. Stiefermann, J. Tschakert, J. E. P. Dahl, R. M. K. Carlson, A. Schirmeisen, P. R. Schreiner, *Nat. Commun.* **2018**, *9*, 2420.

[22] a) B. Mallada, A. Gallardo, M. Lamanec, B. de la Torre, V. Špirko, P. Hobza, P. Jelinek, *Science* **2021**, *374*, 863–867; b) G. Cavallo, P. Metrangolo, R. Milani, T. Pilati, A. Priimagi, G. Resnati, G. Terraneo, *Chem. Rev.* **2016**, *116*, 2478–2601.

[23] a) N. Pavliček, B. Schuler, S. Collazos, N. Moll, D. Pérez, E. Guitian, G. Meyer, D. Peña, L. Gross, *Nat. Chem.* **2015**, *7*, 623–628; b) Q. Zhong, A. Ihle, S. Ahles, H. A. Wegner, A. Schirmeisen, D. Ebeling, *Nat. Chem.* **2021**, *13*, 1133–1139.

[24] L. Lafferentz, V. Eberhardt, C. Dri, C. Africh, G. Comelli, F. Esch, S. Hecht, L. Grill, *Nat. Chem.* **2012**, *4*, 215–220.

[25] S. Kawai, K. Takahashi, S. Ito, R. Pawlak, R. Meier, P. Spijker, F. Canova, J. Tracey, K. Nozaki, A. S. Foster, E. Meyer, *ACS Nano* **2017**, *11*, 8122–8130.

[26] a) S. Yu, A. Noble, R. B. Bedford, V. K. Aggarwal, *J. Am. Chem. Soc.* **2019**, *141*, 20325–30334; b) M. Mato, A. Franchino, C. Garcia-Morales, A. M. Echavarren, *Chem. Rev.* **2021**, *121*, 8613–8684.

[27] W. Auwärter, D. Écija, F. Klappenberger, J. V. Barth, *Nat. Chem.* **2015**, *7*, 105–120.